Static and Dynamic Properties of Optical Microcavities in Photonic Bandgap Yarns**

By *Gilles Benoit*, *Shandon D. Hart*, *Burak Temelkuran*, *John D. Joannopoulos*, and *Yoel Fink**

The recent fabrication of fibers surrounded by[1] or lined with[2] alternating layers of materials with a large disparity in their refractive indices presents interesting opportunities for passive and active optical devices. While a periodic multilayer structure, such as the one reported above, leads to the formation of photonic bandgaps and an associated range of high reflectivity,[3,4] it is the incorporation of intentional deviations from periodicity, so called "defects", that allows for the creation of localized electromagnetic modes in the vicinity of the defect. These structures, sometimes called optical cavities, in turn can provide the basis for a large number of interesting passive and active optical devices, such as vertical cavity surface-emitting lasers (VCSELs),[5] bi-stable switches,[6] tunable dispersion compensators,[7] tunable drop filters,[8] and more. In this paper, we report on the fabrication of a fiber surrounded by a Fabry–Perot cavity structure and demonstrate that by application of axial mechanical stress, the spectral position of the resonant Fabry–Perot mode can be reversibly tuned.

The optomechanical tuning behavior of multilayer dielectric structures has been studied by Kimura et al. who reported a normalized reversible shift (defined as the shift in wavelength $\Delta\lambda$ normalized by the wavelength λ) of 3.4 % under a load of 18.5 kg mm^{-2} applied perpendicular to an all-polymer multilayer reflector.[9] Fiber Bragg gratings (FBGs) have been tuned mechanically using piezoelectric transducers (PZTs) to generate strains perpendicular to the grating leading to normalized shifts as high as 2.9 % under 1000 V.[10] A normalized shift of 0.64 % under 50 V is the highest tuning efficiency reported to date for tunable FBG filters using PZTs.[11]

Our fabrication technique allows for the accurate placement of optical cavities that can encompass the entire or partial fiber circumference. The fibers discussed in this paper are made of arsenic triselenide (As_2Se_3), a chalcogenide glass, and poly(ether sulfone) (PES) and have a low-index Fabry–Perot cavity (Fig. 1).

This was achieved by introducing an extra polymer layer in the middle of the periodic multilayer structure of the preform, thus generating a defect mode in the photonic bandgaps[3] of the drawn fibers. The position of the bandgap centre is linearly related to the optical thickness of the layers by the Bragg condition.[4] Through accurate outer diameter control afforded by the laser micrometer mounted on the draw tower, we have been able to place gaps (Fig. 2) at wavelengths ranging from 11 μm to below 1 μm. Such cost-effective tunable optical filters could lead to applications such as optical switches for wavelength-division-multiplexing (WDM) systems and sensors.

The cross-sectional structures of a 240 μm and a 460 μm diameter fiber were observed by scanning electron microscopy (SEM) using a backscattered electron detector (Fig. 1). The structure is composed of a hollow core polymer rod surrounded by six bilayers of As_2Se_3 and PES, separated in the middle by an extra polymer layer, which forms the Fabry–Perot cavity. An extra polymer layer protects the fiber surface. For the 240 μm (460 μm) diameter fiber, the glass layers are ~135 nm (255 nm) thick, except for the first and the last ones, which are half as thick; the polymer layers are ~270 nm (510 nm) thick and the defect layer is ~610 nm (1145 nm) thick.

Reflectivity spectra measurements were performed using an infrared microscope (Nicolet SpectraTech NicPlan) and a Fourier-transform infrared spectrometer (Magna 860) using a lens with a 30° collection angle. The spectra exhibited a single-mode Fabry–Perot resonant mode at 1.74 μm and 3.2 μm for the 240 μm and 460 μm diameter fibers, respectively (Fig. 3).

The spectral width of the cavity resonant mode is broadened due to the range of incident angles. Using the different thicknesses and the real and imaginary part of the refractive index (n,k) of As_2Se_3 and PES carefully measured with a broadband (300 nm to 16 μm) spectroscopic ellipsometer (Sopra GES-5), the reflectivity spectra of these fibers were computed with the transfer matrix method (TMM) by approximating them as a one-dimensional planar stacking. By averaging the calculated spectra over the experimental incidence angles and polarizations, we obtained very good agreement between the simulation and the measurements.

We focused our optomechanical analysis on the elastic regime, which ultimately defines the operational tuning range of these fibers. The fiber's Young's modulus (E) can be approximated by modeling this multilayer structure as independent parallel springs under axial (along the z-axis of the fiber)

[*] Prof. Y. Fink, G. Benoit, S. D. Hart, Dr. B. Temelkuran
Department of Materials Science and Engineering
Massachusetts Institute of Technology
Massachusetts Ave., Cambridge, MA 02138 (USA)
E-mail: yoel@mit.edu

Prof. Y. Fink, G. Benoit, S. D. Hart, Dr. B. Temelkuran,
Prof. J. D. Joannopoulos
Research Laboratory of Electronics
Massachusetts Institute of Technology
Massachusetts Ave., Cambridge, MA 02138 (USA)

Prof. J. D. Joannopoulos
Physics Department
Massachusetts Institute of Technology
Massachusetts Ave., Cambridge, MA 02138 (USA)

[**] The authors thank M. Frongillo, Dr. K. Kuriki, T. McLure, Dr. P. Prideaux, and Dr. R. Sun for their help. This work was supported in part by DARPA QUIST (contract number DAAD 19-01-1-0647), the ONR (contract number N00014–02–1–0717), the AFOSR (contract number Y77011), the US DOE, the U.S. Army through the Institute for Soldier Nanotechnologies (contract number DAAD-19–02D-0002), and a NSF Graduate Resarch Fellowship. The content does not necessarily reflect the position of the Government, and no official endorsement should be inferred. This work was also supported by the Materials Research Science and Engineering Center (MRSEC) program of the National Science Foundation under Grant No. 0123460 and made use of the Shared Experimental Facilities supported in part by the MRSEC Program of the National Science Foundation under award number DMR 02–13282.

 DOI: 10.1002/adma.200305585

ADVANCED MATERIALS

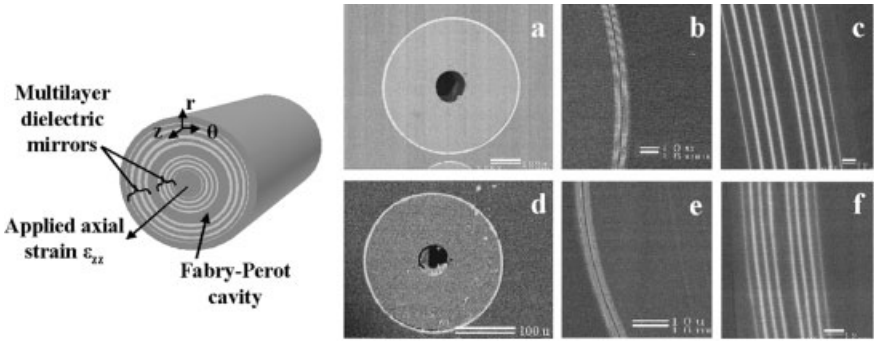

Fig. 1. Schematic of the structure of dielectric mirror fibers made of As_2Se_3 (bright) and PES (in gray) with a low-index Fabry–Perot cavity (the local cylindrical coordinate system is represented as well as the applied axial strain, ε_{zz}), and backscattered SEM images of the cross-sections of a 460 μm (a–c) and a 240 μm diameter fiber (d–f) embedded in epoxy and microtomed. a,d) The entire cross-section of the fibers is shown; b,e) long-range layer uniformity is demonstrated; and c,f) the ordering and adhesion of the Fabry–Perot cavity structure is revealed. Scale bars have been redrawn for clarity.

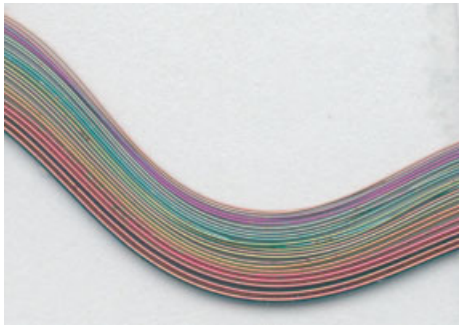

Fig. 2. Array of parallel fibers with outer diameter ranging from ~ 420 μm (bottom) to ~ 100 μm (top). The colors are due to the narrow higher order photonic bandgap in the visible region.

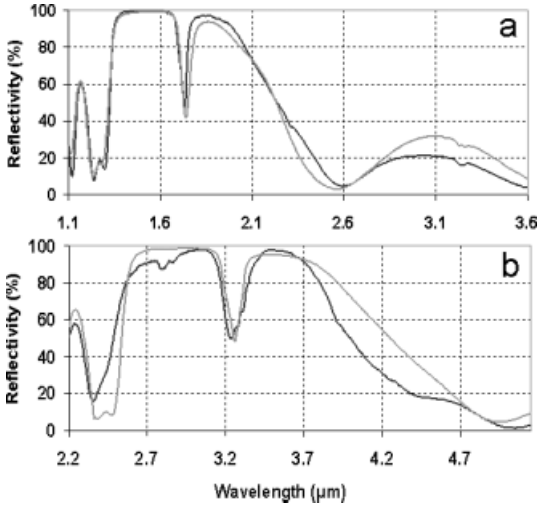

Fig. 3. Computed (gray lines) and measured (black lines) reflectivity spectra for the 240 μm (a) and the 460 μm diameter fibers (b) with Fabry–Perot resonant modes at 1.74 μm and 3.2 μm, respectively.

strain assumed to be equal for all the layers, leading to an effective Young's modulus of 2.64 GPa (using $E_{PES} = 2.4$ GPa for bulk PES[12] and $E_{As_2Se_3} = 15$ GPa reported for 1.5 μm thick films[13]).

Neglecting the possible strain-induced refractive-index variation of the materials, the normalized shift of the Fabry–Perot resonant mode can be related to the applied axial strain by calculating the radial stresses σ_{rr} (resulting from the difference between the Poisson ratios of the materials—$\nu_{PES} = 0.45$[12] and $\nu_{As_2Se3} = 0.289$[13]—and the adhesion condition between the layers) and displacements u_r in each layer under axial strain. Starting from the equilibrium equations and using Hooke's law and Lame's equations, we derive:

$$\frac{\partial \sigma_{zz}}{\partial z} = 0 \tag{1}$$

$$\frac{\partial \sigma_{rr}}{\partial r} + \frac{\sigma_{rr} - \sigma_{\theta\theta}}{r} = 0 \Leftrightarrow \frac{d^2 u_r}{d^2 r} + \frac{1}{r}\frac{du_r}{dr} - \frac{u_r}{r^2} = 0 \tag{2}$$

Solving Equation 2 leads to a general expression for u_r and σ_{rr} with two unknowns A and B per layer:[14,15]

$$u_r = \frac{A}{r} + Br \tag{3}$$

$$\sigma_{rr} = -\frac{2GA}{r^2} + 2(\eta + G)B + \eta\varepsilon_{zz} \tag{4}$$

where

$$G = \frac{E}{2(1+\nu)} \tag{5}$$

is the shear modulus and

$$\eta = \frac{E\nu}{(1+\nu)(1-2\nu)} \tag{6}$$

the Lame modulus. The continuity of the displacement and the radial stress at each interface plus the boundary conditions (σ_{rr} vanishes at free surfaces) can be expressed as a linear system whose unique solution allows us to relate the radial strain in each layer to the applied axial strain as a linear relation $\varepsilon_{rr} = C\varepsilon_{zz}$, where C can be interpreted as an effective Poisson ratio. Finally, taking into account that the Fabry–Perot resonant mode itself is linearly shifted within the bandgap because of the different effective Poisson ratios of the glass and polymer layers, we obtain a linear relation between the normalized shift of the Fabry–Perot resonant mode and the applied axial strain:

$$\frac{\Delta\lambda}{\lambda} = -0.373\varepsilon_{zz} \tag{7}$$

All the layers (except the outer protective polymer layer) are under tensile radial stress whose maximum (0.22 MPa un-

der 1 % axial strain) is located at the interface between the layers and the polymer core where delamination is most likely to occur.

Measurements were performed on ~30 cm long fibers that were fixed at one end with epoxy to a load cell (Transducer Techniques MDB-2.5) while the other end was attached with strong tape to a pole mounted on a stepper rotational stage (Newport PR50; Fig. 4). This end of the fiber was also screwed to the pole to further secure it in place.

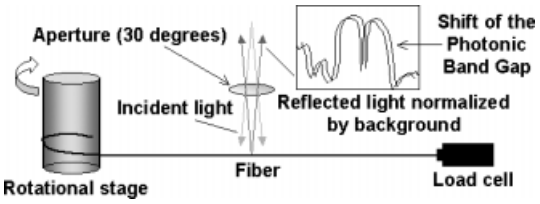

Fig. 4. Experimental set-up used for mechanical tuning demonstration.

The uncertainty on the Young's modulus due to the precision of the load cell was lower than 30 MPa. All the reflectivity spectra were normalized to a background taken with a flat gold mirror and were measured at a fixed reference position on the fiber. The strain measurements were performed by measuring the position of two reference points chosen, as far as possible from the fixed ends of the fiber to avoid errors due to non-uniform strain near the fiber's edges.

By focusing on the resonant mode in the fundamental bandgap of the 240 μm and the 460 μm diameter fiber, we demonstrated the tuning of the Fabry–Perot resonant mode under increasing axial strain (Fig. 5).

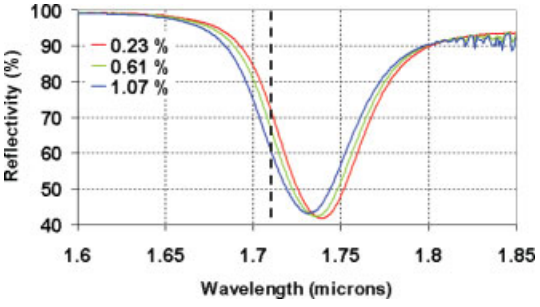

Fig. 5. Reflectivity versus wavelength plot showing the shift of the Fabry–Perot resonant mode of the 240 μm diameter fiber for three increasing values of the applied axial strain.

Due to the shift in the resonant mode position, a change in reflectivity at fixed wavelength occurs, which was found to be 13 % at 1.71 μm (dashed line) for the 240 μm diameter fiber when increasing the applied axial strain from 0.23 % (red line) to 1.07 % (blue line). The normalized-shift versus strain curves (Fig. 6) appeared to be linear for both fibers up to approximately 0.9 % (dashed line) with a slope equal to –0.38 for both the 240 μm and the 460 μm diameter fiber, in good agreement with the predicted value (–0.373, Eq. 7).

The normalized shift was equal to –0.35 % for 0.9 % applied axial strain, which seems to be the limit of the elastic regime

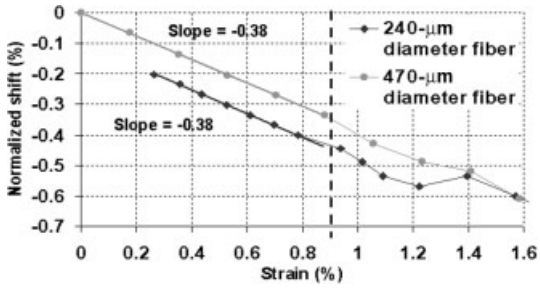

Fig. 6. Normalized shift of the Fabry–Perot resonant mode (defined as $\Delta\lambda/\lambda$) versus applied axial strain for the 240 μm (black diamonds) and the 460 μm diameter fiber (gray circles). The curve obtained for the 240 μm diameter fiber is lower because the experimental "0 %" strain is likely to correspond to a non-zero positive strain, necessary to keep this thinner fiber straight for the measurement (equivalent to a load less than 10 g).

and corresponds to small applied loads: 76 g and 300 g for the 240 μm and 460 μm diameter fiber, respectively. Under higher strains, the normalized shift versus strain curves were not linear anymore and the measured loads would start decreasing slightly with time, which could be a sign of delamination between the layers and the polymer core, of plastic deformation and/or of relaxation in the layers. The stress–strain curves also exhibit an elastic regime up to approximately 1 % strain with a corresponding Young's modulus equal to 2.59 GPa for the 240 μm outer diameter (OD) fiber and to 2.39 GPa for the 460 μm OD fiber. These values are slightly lower than the predicted value, possibly due to humidity and relaxation effects in the polymer and the glass layers (for As_2Se_3 and PES, $T_g = 175\,^{\circ}C$[16] and 220 °C,[12] respectively).

We have demonstrated the fabrication and reversible mechanical wavelength tuning of Fabry–Perot resonance modes in a 240 μm and a 460 μm diameter dielectric mirror fiber. The magnitude of the normalized shift of the cavity mode wavelength was measured to be 0.35 % under a maximum axial strain of 0.9 %. The wavelength change in reflectivity was 13 % over a 30° collection angle. Narrower collection angles will lead to larger changes in reflectivity up to a value of 40 % for this structure. Applications that require an even larger change in reflectivity would necessitate higher quality factors, which can be achieved by increasing the number of bilayers.

Experimental

Materials: PES films were purchased from Goodfellow Corporation. Films were 25 or 50 μm thick. Arsenic triselenide (As_2Se_3) was purchased from Alfa Aesar/Strem Chemicals (purity 99.999 %).

Preform Preparation: 12 cm wide strips of PES were cut, cleaned with methanol, and baked for 5 h at 150 °C under vacuum. The 50 ± 5 μm thick strips were used to build the inner core of the preform by hand rolling them onto a 7 mm diameter borosilicate glass tube (Corning Pyrex) and baking the resulting piece for 6 h at 150 °C under vacuum, while a 25 ± 2 μm thick strip was used to build the layered photonic bandgap structure.

As_2Se_3 was deposited on both sides of the 25 μm polymer film using a thermal evaporator (Ladd Industries). The evaporation was performed using two electrodes under a vacuum kept below 2×10^{-5} torr. The deposition rate was ~100 Å s^{-1} and the targeted thickness was 6 μm, corresponding to a quarter-wave structure. In-situ layer thickness monitoring was carried out using a crystal thickness monitor (Sycon STM100). The area of PES film coated during one

ADVANCED MATERIALS

evaporation was approximately 12 cm × 25 cm. The defect layer was created by the designed placement of a mask on the film during evaporation.

The As_2Se_3 coated PES film was then rolled onto the PES core and the resulting preform, ~2 cm in diameter, was covered with Teflon tape and consolidated at 260 °C (±5 °C) under vacuum for 20 min. The pressure was decreased quickly below 5 torr within the first 5 min. The preform was then quenched in a –20 °C freezer for about 2 min to prevent crystallization and annealed initially at 150 °C and then cooled slowly for ~2 h.

The inner glass tube was then dissolved with HF by immersing the entire preform. After complete etching, the preform was rinsed with distilled water and isopropanol and baked under vacuum at 150 °C for 5 h.

Fiber Drawing: Our draw tower is composed of a three-zone vertical tube furnace (Thermcraft), a motorized capstan (Heathway) to control the speed of the drawing, and laser diameter monitors (Beta LaserMike) to monitor the outer diameter of the drawn fiber. The temperature of the upper, central, and lower zones of the oven were typically around 240 °C, 295 °C, and 150 °C, respectively, for speeds ranging between ~1–10 m s^{-1}.

SEM: SEM was performed on small sections of fibers embedded in epoxy resin, cut by ultramicrotome (Ultracut E, Reichert-Jung) with a diamond knife to obtain a smooth surface, and gold coated using a (Denton Vacuum) sputtercoater (~10 nm thick gold coating). We used a JEOL 6320 FEGSEM with backscattered detector at 10 keV to obtain a good contrast between the PES and As_2Se_3 layers.

Ellipsometry Measurements: The refractive indices (n,k) of As_2Se_3 and PES were measured with a broadband spectroscopic ellipsometer (Sopra GES-5) utilizing three different detectors: photomultiplier from 250 nm to 880 nm, InGaAs from 880 nm to 2 μm, and MCT-A from 2 μm to 20 μm. Corrections were used to account for the nonlinearities and polarization dependence of the detectors. The samples consisted of a film deposited on silicon substrate. As_2Se_3 films were deposited by thermal evaporation (similarly to the fiber fabrication process) and annealed for 1 h at 180 °C, whereas PES films were spin coated (Laurell Tech. Corp. WS-400 A-6 NPP/LITE) at 1500 rpm (rpm = revolutions per minute) from a polymer solution obtained by dissolving a 25 μm PES film (Goodfellow) in *N*,*N*-Dimethylformamide. For each sample, the ellipsometric parameters $\tan\Psi$ and $\cos\Delta$ parameters were fitted to extract the thickness of the deposited film and to calculate n and k versus wavelength using the Levenberg–Marquardt regression method with a Cauchy-like dispersion relation and additional Lorentzian absorption peaks for PES.

Fourier-Transform Infrared Spectrometer (FTIR) Measurements: Reflectivity measurements were performed using a infrared microscope (Nicolet Spectra-Tech NicPlan) and a FTIR (Magna 860). All backgrounds were taken using a flat gold mirror. Reflectivity spectra were normalized by a factor of ~1.1 to correct assumed differences between the fiber and flat background mirror geometry.

Mechanical Tuning: The precision of the load cell (Transducer Techniques MDB-2.5) was equal to 1 mg, the precision of the stepper rotational stage (Newport PR50) was equal to 0.1°, and the diameter of the pole was equal to 2.1 cm. The whole setup was placed on the motorized stage of the microscope, whose accuracy was ~1 μm. Reference positions on the fibers were taken as surface defects of the order of 2 or 3 μm in diameter, larger than the resolution of the motorized stage.

Simulations: All computations were performed using Matlab.

Received: June 23, 2003
Final version: September 24, 2003

[1] S. D. Hart, G. R. Maskaly, B. Temelkuran, P. H. Prideaux, J. D. Joannopoulos, Y. Fink, *Science* **2002**, *296*, 510.
[2] B. Temelkuran, S. D. Hart, G. Benoit, J. D. Joannopoulos, Y. Fink, *Nature* **2002**, *420*, 650.
[3] J. D. Joannopoulos, R. D. Meade, J. N. Winn, in *Photonic Crystals—Molding the Flow of Light*, Princeton University Press, Princeton **1995**.
[4] P. Yeh, in *Optical Waves in Layered Media* (Ed: J. W. Goodman), John Wiley & Sons, Inc., New York **1988**.
[5] M. Bugajski, J. Muszalski, B. Mroziewicz, K. Reginski, T. J. Ochalski, *Opt. Appl.* **2001**, *31*, 273.
[6] M. Soljacic, M. Ibanescu, S. G. Johnson, Y. Fink, J. D. Joannopoulos, *Phys. Rev. E* **2002**, *66*.
[7] Y. W. Song, D. Starodubov, Z. Pan, Y. Xie, A. E. Willner, J. Feinberg, *IEEE Photonic Technol. Lett.* **2002**, *14*, 1193.
[8] Y. N. Zhu, C. Lu, B. M. Lacquet, P. L. Swart, S. J. Spammer, *Opt. Commun.* **2002**, *208*, 337.
[9] M. Kimura, K. Okahara, T. Miyamoto, *J. Appl. Phys.* **1978**, *50*, 1222.
[10] H. G. Limberger, A. Iocco, R. P. Salathe, L. A. Everall, K. E. Chisholm, I. Bennion, *25th European Conf. Optical Commun. (ECOC 1999)*, IEEE, Piscataway, NJ **1999**.
[11] T. Inui, T. Komukai, M. Nakazawa, *Opt. Commun.* **2001**, *190*, 1.
[12] J. E. Mark, in *Polymer Data Handbook* (Ed: J. E. Mark), Oxford University Press, New York **1999**.
[13] T. N. Shchurova, N. D. Savchenko, *J. Optoelectron. Adv. Mater.* **2001**, *3*, 491.
[14] Z. Hashin, B. W. Rosen, *J. Appl. Mech.* **1964**, 223.
[15] R. M. Jones, in *Mechanics of Composite Materials*, McGraw-Hill, New York **1975**.
[16] Z. U. Borisova, in *Glassy Semiconductors*, Plenum Press, New York **1981**.

Optical and Electronic Contributions in Double-Heterojunction Organic Thin-Film Solar Cells**

By *Helmut Hänsel*, *Heiko Zettl*, *Georg Krausch*,* *Roman Kisselev*, *Mukundan Thelakkat*, and *Hans-Werner Schmidt*

Different studies have shown that the introduction of additional functional layers in donor/acceptor organic solar cells can enhance the performance significantly.[1–5] TiO_2 has been proven to serve as an exciton dissociation surface,[3] poly(3,4-ethylene dioxythiophene):poly(styrene sulfonate) (PEDOT:PSS) has been found to facilitate hole injection and to increase the built-in potential;[5,6] in organic light-emitting diodes (OLEDs) it has been shown to also hinder oxygen-induced aging at the indium tin oxide (ITO) electrode.[7,8] LiF is used as an electron injector in combination with an aluminum cathode, and bathocuproine (BCP) has been shown to be an efficient exciton blocking layer in both, photovoltaic cells[4,5] and OLEDs.[9] In our own experiments,[10,11] an additional TiO_2 layer resulted in higher efficiencies of single-heterojunction organic solar cells. Until now, the function of this layer has not been understood quantitatively. Both an electronic and an optical effect were proposed as possible explanation; however, there were no means to determine their relative importance. For polymer/C_{60} and CuPc/C_{60} (CuPC = copper phthalocyanine) heterojunction cells, it has been shown by layer thickness variation that the light intensity at the heterojunction determines the photocurrent and that interference with the light reflected from the electrode has to be taken into account.[12,13] A comparison of the experimental data with predictions from a standing wave argument led to good agreement in the periodicity of the photocurrent. Electronically, the interface morphology, exciton diffusion, charge-carrier

[*] Prof. G. Krausch, H. Hänsel, H. Zettl
Physikalische Chemie II
Universität Bayreuth
D-95440 Bayreuth (Germany)
E-mail: georg.krausch@uni-bayreuth.de
Prof. G. Krausch, H. Hänsel, H. Zettl
Bayreuther Zentrum für
Kolloid und Grenzflächenforschung (BZKG)
D-95440 Bayreuth (Germany)
R. Kisselev, Dr. M. Thelakkat, Prof. H.-W. Schmidt
Makromolekulare Chemie I and Bayreuther Zentrum für
Kolloid und Grenzflächenforschung (BZKG)
Universität Bayreuth
D-95440 Bayreuth (Germany)

[**] The research project was funded by the German Science Foundation DFG (SFB 481).

  DOI: 10.1002/adma.200305274 *Adv. Mater.* **2003**, *15*, No. 24, December 17